Numerical Study on Flow Characteristics at Blade Passage and Tip Clearance in a Linear Cascade of High Performance Turbine Blade

Hyon Kook Myong*
School of Mechanical and Automotive Engineering, Kookmin University, Seoul 136-702, Korea
Seung Yong Yang
Department of Mechanical Engineering, Graduate School, Kookmin University, Seoul 136-702, Korea

A numerical analysis has been conducted in order to simulate the characteristics of complex flow through linear cascades of high performance turbine blade with/without tip clearance by using a pressure-correction based, generalized 3D incompressible Navier-Stokes CFD code. The development and generation of horseshoe vortex, passage vortex, leakage vortex, tip vortex within tip clearance, etc. are clearly identified through the present simulation which uses the RNG k-ε turbulent model with wall function method and a second-order linear upwind scheme for convective terms. The present simulation results are consistent with the generally known tendency that occurs in the blade passage and tip clearance. A 3D model for secondary and leakage flows through turbine cascades with/without tip clearance is also suggested from the present simulation results, including the effects of tip clearance height.

Key Words : Turbine Cascades, Tip Clearance, Secondary Flow, Leakage Flow, Leakage Vortex, Tip Vortex, Simulation

1. Introduction

The leakage flow passing through tip clearance is one of the most prevalent and influential features of the flow through turbomachine rotors. The most significant effects of tip leakage flow and its associated vortex are blockage of the passage flow, aerothermal losses associated with resulting secondary flows and complexities in blade heat transfer. In addition, tip leakage flow is a phenomenon that is difficult to either predict or measure particularly in axial turbines. Thus, for the optimal design of turbine it is crucial to understand flow characteristics at the blade passage and the tip clearance.

There have been numerous experimental and numerical studies to understand and describe the complex flow fields inside a turbine blade passage. For example, an extensive review of both experimental and numerical studies of tip leakage flow in axial flow turbines can be found in the lecture series by Sjolander (1997) and a review of early numerical simulation studies of turbomachines is given in the text by Lakshminarayana (1996). A brief review of numerical and experimental studies of tip leakage flow that are relevant to this paper is given here, including more recent studies for completeness. Langston et al. (1977) and Langston (1980) first suggested a secondary flow model through the extensive and detailed experimental study of the flow field in a

* Corresponding Author,
E-mail : myong@kookmin.ac.kr
TEL : +82-2-910-4714; **FAX** : +82-2-910-4839
School of Mechanical and Automotive Engineering, Kookmin University, Seoul 136-702, Korea. (Manuscript **Received** July 8, 2002; **Revised** November 27, 2002)

large scale linear turbine cascade. Thereafter, several numerical studies were performed. Hah (1984) analyzed a three-dimensional turbulent flow inside turbine blade rows using an algebraic Reynolds stress model modified for effects of the streamline curvature and rotation. Yoo and Yun (1994) performed a numerical study by using the standard k-ε turbulence model, and compared with the experimental data of Langston et al. (1977). They found that the second order linear upwind scheme gave better agreement with the experimental results than the usual upwind scheme. Yamamoto (1989) measured a tip clearance flow field, clearly showing very high tip leakage flow and its roll-up into a vortex, including interaction with the secondary flow. Lee (1995) used the RNG k-ε turbulence model to calculate turbulent flows for the turbine blade studied experimentally by Yamamoto (1989), and showed that the RNG model was more accurate than the standard k-ε turbulence model to predict saddle point, horseshoe vortex and passage vortex. Basson and Lakshminarayana (1995) performed a numerical study for the linear cascade with moderate turning blade with the low-Reynolds k-ε turbulence model of Chien(1982) and compared with the experimental data studied by Bindon and Morphis (1992). Chernobrovkin (1999) also computed the flow through a turbine with moderate turning and found that the leakage vortex began at an axial location of 50% chord, but roll-up did not occur until about 80% chord. Recently, Tallman and Lakshminarayana (2000) used additionally the Lagrangian method to show the particle traces of leakage flow and its associated vortex in order to understand their detailed flow physics. In particular, they reported that vortex roll-up began at between 30% and 40% of the axial distance from the leading edge, which was in contrast with the result of Chernobrovkin (1999).

The suction leg of the horseshoe vortex is still another issue to be open to debate. Langston et al. (1977) and Langston (1980) observed that the suction leg of the horseshoe vortex (which was opposite in direction to passage vortex) continued on the suction side. In contrast, Klein (1966) showed through the experimental study that the suction leg of the horseshoe vortex diffused and dissipated by the time it reached the trailing edge. Ho and Lakshminarayana (1994) reported through their computational simulation that the horseshoe vortex diffused and dissipated quickly.

The general objective of the present paper is to study the tip leakage flow and its resulting vortex in order to add to their general understanding for a linear cascade of high performance turbine blade. This understanding includes knowledge of the leakage flow's direction, pressure gradient, leakage vortex and its roll-up etc. In addition, we try to find more accurate and economical calculation method through the present study. Thus, a numerical analysis has been conducted in order to simulate the flow characteristics through a linear cascade of high performance turbine blade with and without tip clearance, which has been studied experimentally by Cho et al. (2001). The Lagrangian method is used to show the particle traces of leakage flow and its associated vortex in order to understand their detailed flow physics. Note here that the present cascade of high performance turbine blade is closer to real one than that with moderate turning blade studied by Tallman and Lakshminarayana (2000).

2. Numerical Technique

The full Reynolds averaged Navier-Stokes equations are employed to model the flow through a linear turbine cascade in the present study. A 3D incompressible Navier-Stokes CFD code (MOSA3D) developed by the authors is used with implementation of cyclic boundary condition. This code is based on the body-fitted coordinate system, pressure-correction and finite volume method (Myong et al., 1996). The RNG k-ε turbulence model with a wall function method and a second-order linear upwind scheme for convective terms are used in the present study to find more accurate and economical calculation method.

Figure 1 shows the nomenclature and the geometric data of the high performance turbine blade. The computational mesh and boundary

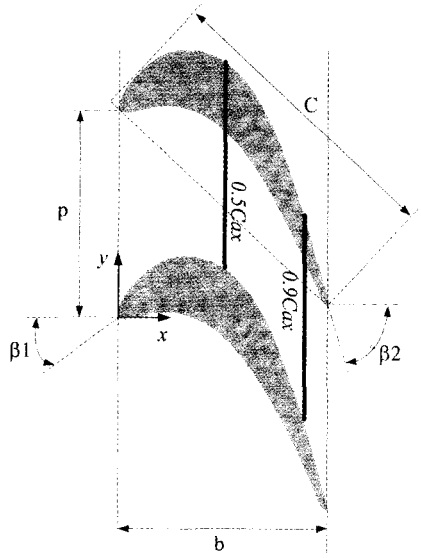

Chord length of blade (C)	: 160 mm
Pitch to Chord ratio (p/C)	: 0.7
Axial Chord to Chord ratio (b/C)	: 0.704
Aspect ratio (l/C)	: 1.21875
Blade inlet angle (β_1)	: 35 deg.
Blade outlet angle (β_2)	: −72.5 deg

Fig. 1 Blade arrangement and geometic data

conditions used in the present study are given in Fig. 2. The computation uses 119 nodes in axial and 34 nodes in pitchwise direction, and 45, 48 and 51 nodes are used for tip clearance cases of 0%, 1.41%, and 2.85% blade span in spanwise direction, respectively. In particular, grid points are clustered near the tip, with 5 and 8 nodes for tip clearance cases of 1.41% and 2.85% span, respectively.

For the wall function to be effective, the dimensionless normal distance y^+ from the wall is considered as follows; at mid-span, the first nodes on both pressure and suction sides are positioned at distance of 30~90 y^+ units from the wall with exception of the leading and trailing edges. Also on both hub wall and shroud, y^+ lies approximately in the range of 30 to 100.

The inlet boundary plane is situated 1.7 times of axial chord length upstream of the leading edge, in a direction parallel to the inlet flow as shown in Fig. 2. The inlet flow condition is a turbulent profile approximated by Prandtl's one-seventh power law, with the free stream velocity

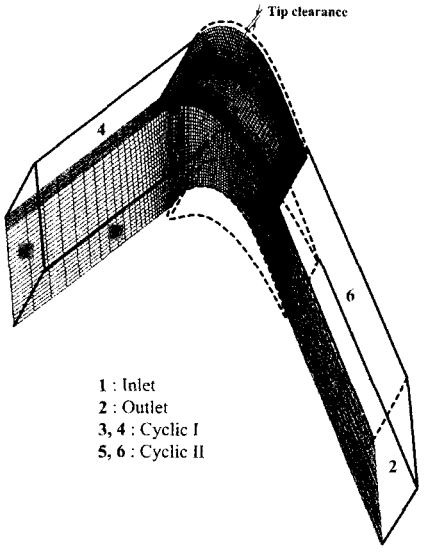

Fig. 2 Mesh (119×34×48) and schematic diagram of boundary conditions

(U_{in}) of 8 m/s, the boundary thickness (δ) of 15 mm, and turbulent intensity of 0.7%. The outlet boundary plane is situated 2.2 times of axial chord length downstream of the trailing edge, in a direction parallel to outlet flow.

A thorough validation of the numerical procedure's ability to resolve turbomachinery flows has been carried out previously by authors for the cascade studied experimentally by Langston et al. (1977) and Langston (1980). For the sake of brevity, validation results are not presented in this paper.

3. Results and Discussions

3.1 Flow through turbine cascades without tip clearance

The flow simulation through turbine cascades without tip clearance is first conducted. The simulation predicted outlet mean flow velocity as 20.81 m/s. The relative difference is about 4%, compared with that of 20 m/s measured experimentally by Cho et al. (2001).

Figure 3 shows the predicted static pressure coefficient distributions on the suction and pressure passage surfaces at 50% span, where the present results are compared with experimental results (Cho at al., 2001). The static pressure

coefficient C_{ps} is defined as follows :

$$C_{ps}=\frac{p_s-p_{t,ref}}{0.5\rho U_{in}^2} \quad (1)$$

where U_{in} is the inlet mean velocity, and p_s and p_t denote the static and total pressures, respectively. Note that the location of the stagnation point here is arbitrarily taken to be the position that yields the best agreement with the experimental results. On both pressure and suction surfaces, there is excellent agreement between the experimental and predicted results.

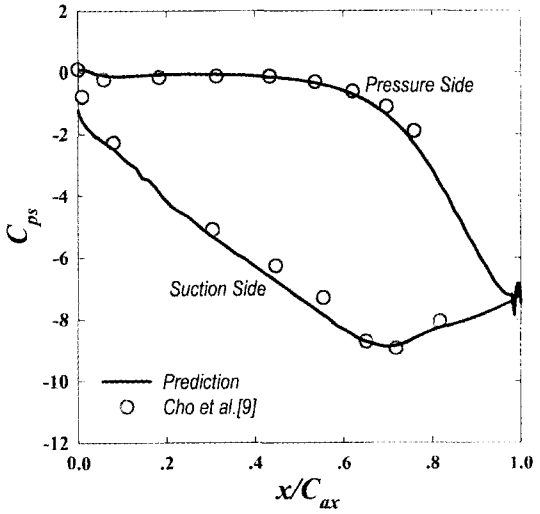

Fig. 3 Static pressure coefficient distributions on blade surfaces (50% span)

Figure 4 shows the predicted velocity vectors, streamlines, and static pressure coefficient distributions on the blade-to-blade plane located at 0.6% span from the endwall (shroud). It can be seen from Fig. 4(a) and (b) that the inlet wall boundary layer separates and forms a horseshoe vortex near the leading edge with one leg of vortex in one blade passage and the other leg in the adjacent passage. The present results from Fig. 4(c) also clearly show a strong negative pressure gradient toward the suction surface in a direction parallel to the separated streamline. This is the region of formation of the horseshoe vortex that originates at the saddle point of separation S and that eventually interacts with the blade suction surface, as shown in Fig. 4(b). Because of this vortex motion in the passage and the secondary flows from various origins (pres-

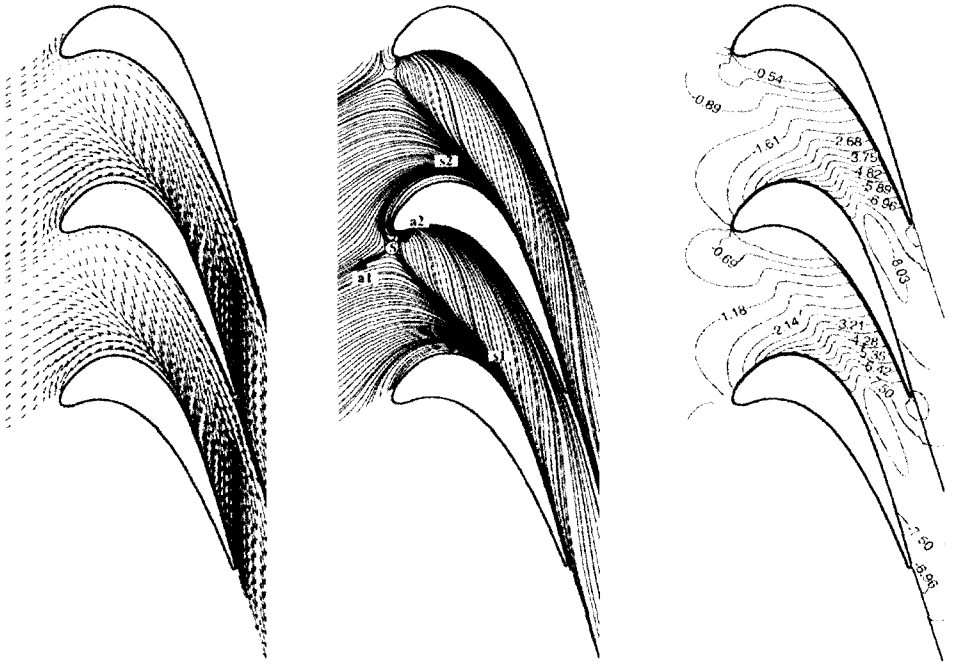

(a) velocity vector (b) streamlines (c) static pressure coefficient

Fig. 4 Flow field in the 0.6% span from the endwall for cascades without tip clearance

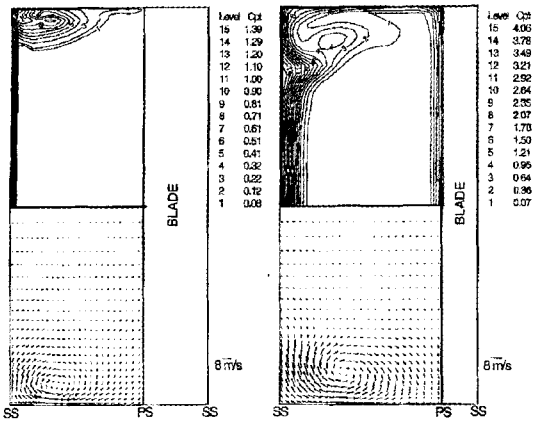

(a) $x=0.5C_{ax}$ (b) $x=0.9C_{ax}$

Fig. 5 Total pressure loss coefficient distributions and secondary flow vectors along the axial direction for a cascade without tip clearance

sure-driven, etc.), large amounts of crossflow are generated. In addition, as shown in Fig. 4(c), the minimum endwall static pressure occurs in the passage near suction side, due to strong secondary flow activity (see Fig. 5), and this low-pressure region indicates the trajectory of secondary vortex. Local maximum static pressure is also observed near the separation saddle point. On the whole, the present results are excellently consistent with the experimental results of Langston et al. (1977), i.e., one leg of a vortex forms behind S-$s1$ from the saddle point and along the suction surface, and the other behind S-$s2$ wrapping around the leading edge and then into the adjacent passage.

Figure 5 shows distributions of total loss coefficient and secondary flow velocity vector in axial planes of 0.5 C_{ax} and 0.9 C_{ax} (see Fig. 1). The total loss coefficient C_{pt} is calculated from the following definition:

$$C_{pt}=\frac{p_{t,ref}-p_t}{0.5\rho U_{in}^2} \tag{2}$$

Note that secondary velocity is obtained from decomposing the total velocity in the x-y plane into 2D streamwise and normal components and then projecting the secondary component into the y-z plane. Thus, the plot of velocity vector components is deviation from potential flow. The magnitude of inlet velocity vector is, for reference, shown alongside of the figure as a scale factor.

In the axial plane of 0.5 C_{ax} (Fig. 5(a)), the horseshoe vortex leg from the saddle point is positioned directly in the suction surface endwall corner and has been considerably reduced in size. However, in the axial plane 0.9 C_{ax} (Figure 5 (b)), before the exit plane of the blade, all of the endwall boundary layer is seen to be very thin. It can be also seen that the passage vortex has grown greatly in size, with the fluid from the inlet boundary layer at its center, and also high losses appear on the endwall near the suction corner where the endwall boundary layer separates and on the suction surface at the separation line where the passage vortex interacts with the suction side boundary layer. In particular, Fig. 5(b) shows clearly that, for the high performance turbine blade the suction side of the horseshoe vortex (which is opposite in direction to passage vortex) continues on the suction side until it reaches the trailing edge, which has been observed by Langston et al. (1977). Note here that, for the turbine blade with moderate turning the suction leg of the horseshoe vortex is commonly known to diffuse and dissipate quickly with no trace of it at 0.8 C_{ax} (Gregory-Smith and Cleak, 1992). Thus, in the case of high performance turbine blade both passage and horseshoe vortices dominate the flow near the suction surface, and due to their formation, the total loss coefficient near the suction side is largely affected.

3.2 Flow through turbine cascades with tip clearance

Now, the simulation results for the flow through turbine cascades with tip clearance are presented and discussed below.

Figure 6 shows the distributions of secondary flow velocity vector and total pressure loss coefficient at $x=0.9$ C_{ax} for the tip clearances of 1.41% and 2.85% span (see Fig. 1). In both cases, the rolled-up leakage vortex is clearly visible near the suction side of the gap as shown in Fig. 6(a). These leakage vortices are seen to extend across about half of the blade spacing, and influence roughly 10% of the blade span closest to the shroud. In particular, the leakage vortex in the

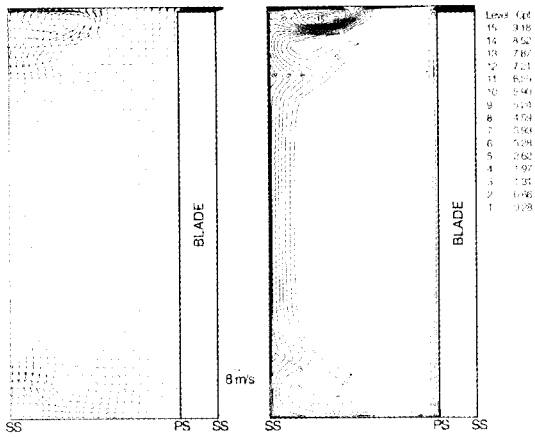

(a) tip clearance case of 1.41% span

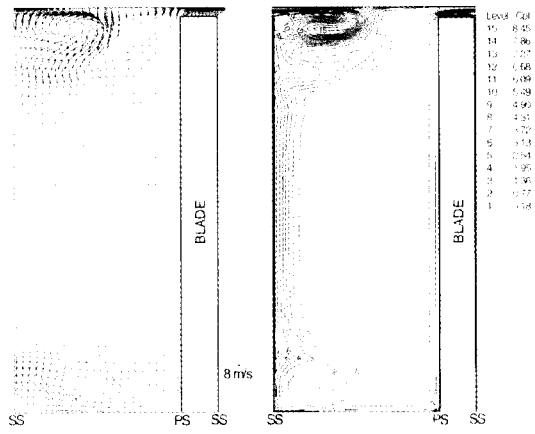

(b) tip clearance case of 2.85% span

Fig. 6 Secondary flow vectors and total pressure loss coefficient distributions at $x=0.9\ C_{ax}$ with tip clearances of 1.41% and 2.85% span

2.85% span case has clearly two loss cores as shown in Fig. 6(b) and is further away from the shroud than the leakage vortex in the 1.41% span case, mainly due to greater mass flow through the gap. Both cases also show a separated flow region at the pressure/tip corner where the flow is turned rapidly into the gap, indicating the strong possibility of tip vortex generation.

The leakage vortex is found to act as an obstruction to the passage flow in both cases. The passage flow near the suction surface is forced underneath and to the side of the leakage vortex, resulting in an additional secondary flow referred to as the blockage secondary flow (Tallman and Lakshminarayana, 2000) and is directed towards the negative spanwise direction. Figure 6 also shows that, as the passage flow is entrained into the gap, it acquires a secondary component of velocity directed towards the pressure surface and towards the blade tip. This secondary flow from the passage towards the gap region is referred to as the gap entrainment secondary flow (Tallman and Lakshiminarayana, 2000). In particular, the present simulation result indicates that, even in flow through cascades with the tip clearance, the suction leg of the horseshoe vortex continues on the suction side until it reaches the trailing edge. On the whole, the size of the leakage vortex as well as the gap entrainment and blockage secondary flows is seen to be clearly larger in the 2.85 % case, mainly due to greater mass flow through the gap.

In Fig. 6(b), the highest total pressure loss region is associated with the leakage vortex and entrainment of fluid around it. Although the high loss region associated with the tip leakage flow is larger in size in the 2.85% span case, the 1.41% span case shows higher total pressure loss values overall in the leakage vortex. The leakage and horseshoe vortices in both cases entrain fluid of higher total pressure around those near the blade suction surface. In addition, the total pressure loss in the leakage vortex core is more than that inside the gap in both cases, indicating that losses are mainly occurring inside the leakage vortex.

Figures 7 and 8 show the predicted velocity vectors, streamlines and static pressure coefficient distributions on the blade-to blade plane located at mid-gap with the tip clearances of 1.41% and 2.85% span, respectively. Along the interface of the leakage jet and passage flows, it can be seen clearly a line indicating division between the leakage and passage flows. The flow through the gap is very similar in magnitude and direction for the two cases, although the 2.85% span case is larger in magnitude and more severely bended than the 1.41% span case. The flow through the gap indicates that the leakage flow is not driven by the pressure difference between the pressure and suction surfaces at a given axial location, which is commonly used in modeling of the leakage velocity. Instead, the leakage fluid that enters the gap near the leading edge directs itself

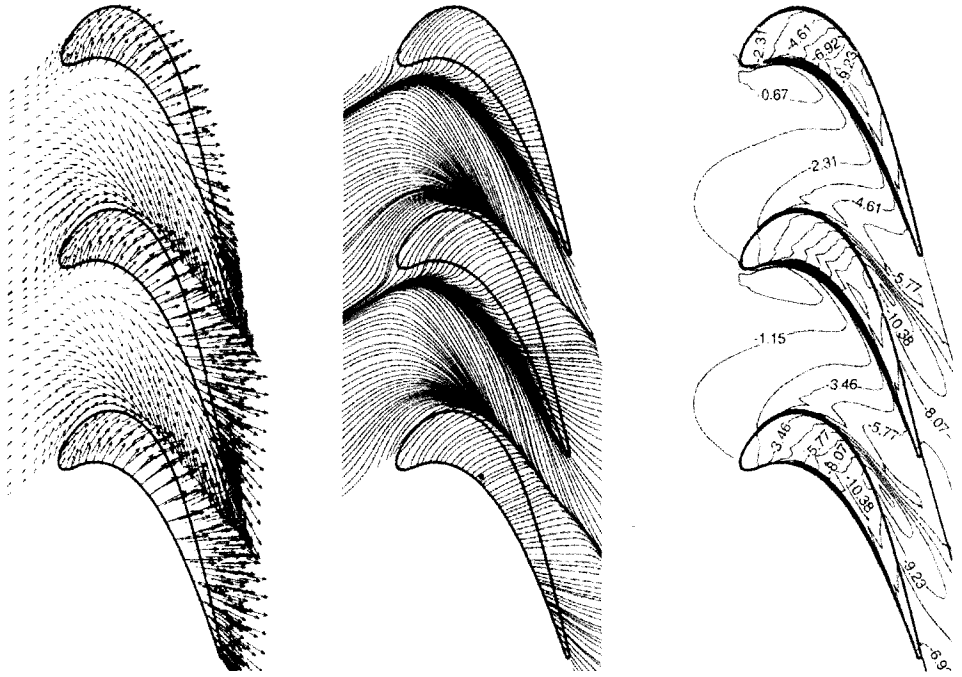

(a) velocity vector (b) streamlines (c) static pressure coefficient

Fig. 7 Flow field at mid-gap (99.4% span) for tip clearance of 1.41% span

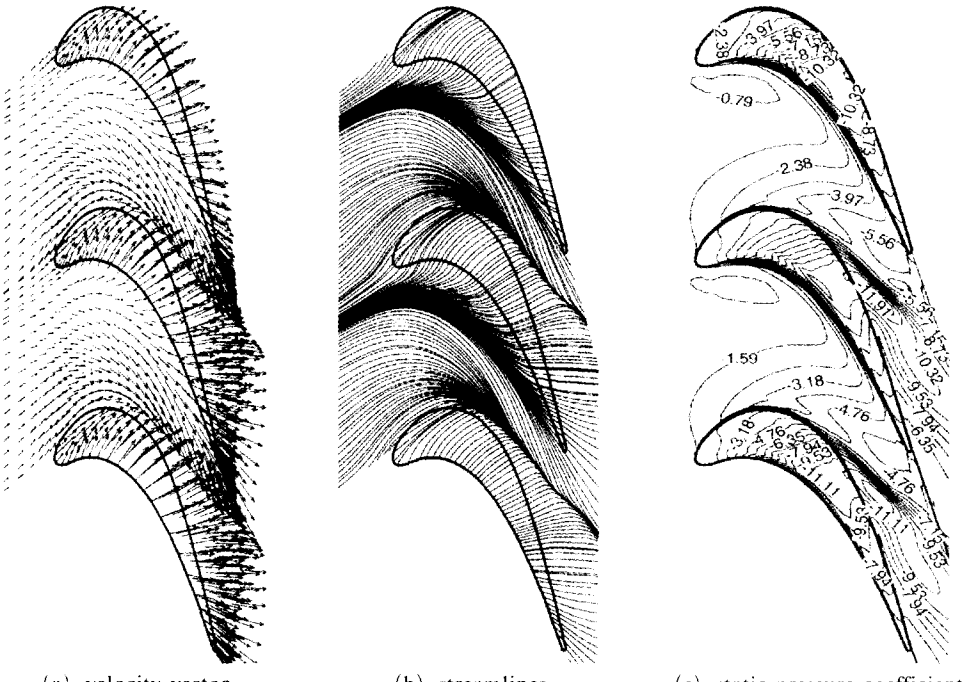

(a) velocity vector (b) streamlines (c) static pressure coefficient

Fig. 8 Flow field at mid-gap (99.02% span) for tip clearance of 2.85% span

both tangentially and axially across the gap in both cases, as it sees lower pressure values in that direction in Figs. 7(c) and 8(c). The leakage fluid that enters the gap further downstream of the leading edge follows a similar trend, but is obstructed by the adjacent leakage fluid. For this cascade of high performance turbine blade, the minimum pressure on the suction surface is located at approximately 75% axial chord in the 1.41% span case and 90% in the 2.85% span case, respectively.

The leakage flow from the gap begins to obstruct the passage flow a little downstream of the blade leading edge in both cases. The severity of the underturning of the flow between the blade suction surface and the interface is roughly the same for the two cases. The size of the underturned region at the passage exit is roughly two-third of the blade spacing for the two cases.

The path of the leakage vortex is also seen from Figs. 7(c) and 8(c) as a region of low pressure propagating from the downstream one-third of the blade in both cases, since the pressure in the vortex becomes low primarily due to swirling motion of the vortex. The low-pressure region of leakage vortex is found to be larger and oriented less parallel to the suction surface in the 2.85% span case than in the 1.41% span case.

The unloading of the blade pressure surface can be also seen near the tip. For both cases, the pressure distribution away from the gap region does not differ significantly from the data at the blade mid-span (see Fig. 9). Near the pressure surface, however, the pressure at the tip decreases with proximity to the gap region. This decrease in pressure is associated with the secondary flow due to gap entrainment, and extends further out from the gap region. The present results are generally consistent with those of Tallman and Laksiminarayana (2000).

Figure 9 shows the pressure coefficient distributions on blade surfaces at 50%, 87%, 96% and 97% spans, for the tip clearance of 2.85% span case. Note that those for the tip clearance of 1.41% span case have a similar trend. The results indicate the characteristics of flow occurring around the tip region. Along the pressure surface the pressure distributions vary with the spanwise location in the range of 0 to 0.9 C_{ax}, with the higher spanwise location, the lower pressure distribution. Thus, the pressure gradient is formed in the spanwise direction. For this reason, the flow is drawn into the tip clearance region. In contrast to the pressure surface, the pressure distributions along the suction surface vary complicatedly with the spanwise location due to the leakage flow, its vortex and the horseshoe vortex along the suction surface. The pressure distribution in the passage near the suction surface side of the gap is fairly constant in the spanwise direction location in the range of 0 to 0.3 C_{ax} and exhibits a largely positive gradient in the pitchwise direction (see Fig. 8). Therefore, the leakage flow, while driven by a pressure drop across the gap, is separated from the tip and merges the main streamwise flow along the suction surface. However, in the range of 0.3 C_{ax} to 0.6 C_{ax}, the pressure distribution decreases with the spanwise location especially near the gap, and the leakage flow separated from the gap quickly encounters an adverse pressure gradient as shown in Fig. 8. Consequently, the leakage flow turns towards the positive spanwise direction. This initiates the leakage vortex roll-up at an axial

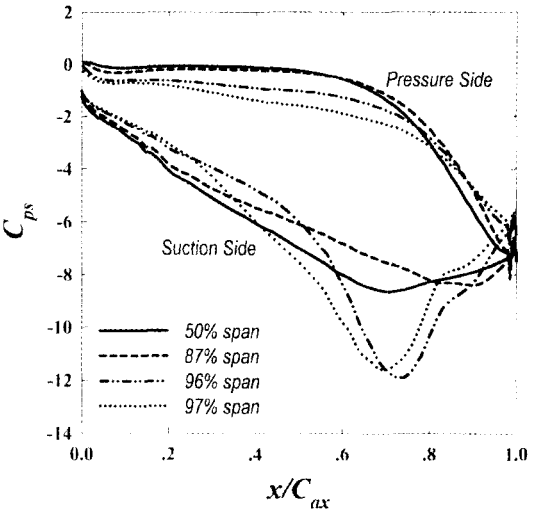

Fig. 9 Static pressure coefficient distributions on blade surfaces for the tip clearance of 2.85% span

location of about 30% chord and makes the helical type of roll-up further downstream. The present result is consistent with the result of Tallman and Lakshminarayana (2000). On the contrary, in the range larger than 0.6 C_{ax}, the pressure distribution increases with the spanwise location especially near the gap, which may make the horseshoe vortex continue on the suction side.

Figure 10 shows fluid pathlines (particle traces) that pass through the tip clearance for both 1.41% and 2.85% tip clearance cases. The origins of the fluid pathlines for two cases are shown in the figure. The results show that the generic structure of the leakage vortex is generally very similar for the two cases. The core of the leakage vortex is composed of fluid that passes through the gap from the leading edge and mid chord regions and near to the blade tip. The leakage vortex begins to roll up at an axial location of about 30% chord and makes the helical type of roll-up further downstream (Fig. 10(a)). The core of leakage vortex also becomes more distant from the suction side. On the contrary, the leakage fluid pathlines passing through the downstream half of the gap are seen to wrap around an existing vortex core without roll-up on their own (Fig. 10(b)). Figure 10 also clearly shows that the tip vortex occurs in the tip near the pressure surface downstream half of the blade for both cases. This tip vortex, with low pressure inside the core, causes cavitation in liquid-handling machinery, which may result in decreased efficiency, and blade tip damage.

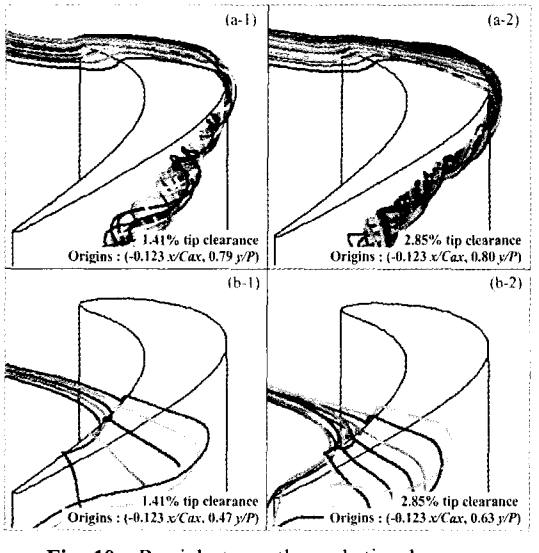

Fig. 10 Particle trace through tip clearance

3.3 Three-dimensional model for flow through turbine cascade

The following three-dimensional model for flow through a linear turbine cascade of high performance turbine blade with and without tip clearance may be obtained as shown in Fig. 11, considering altogether the results presented herein.

In the case of the turbine blade without tip clearance, the horseshoe vortex formation occurs near the leading edge. The suction side leg of the horseshoe vortex continues on the suction side and the pressure side leg of the horseshoe vortex moves toward the suction side after it enters the passage. Then the pressure side of horseshoe vortex merges with the passage vortex near the suction surface, since both have the same sense of rotation. On the contrary, the suction side of the horseshoe vortex (which is opposite in direction to passage vortex) continues on the suction side until it reaches the trailing edge.

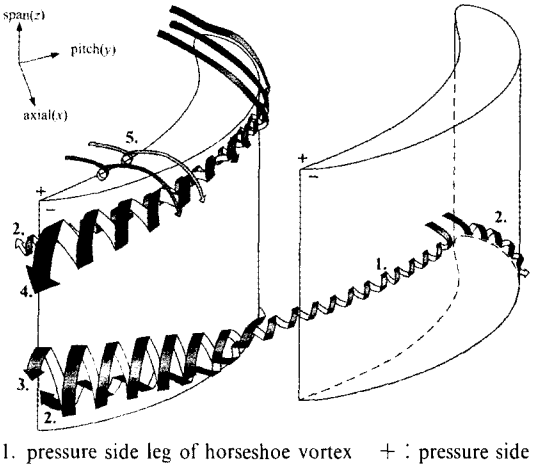

1. pressure side leg of horseshoe vortex
2. suction side leg of horseshoe vortex
3. passage vortex
4. leakage vortex
5. tip vortex

+ : pressure side
− : suction side

Fig. 11 Pattern for secondary and leakage flows through turbine cascades

In the case of the turbine blade with tip clearance, the core of leakage vortex is composed of fluid that passes through the gap from the leading edge and mid chord regions and near to the blade tip. The leakage vortex begins to roll up at about 30% of the axial distance from the leading edge and makes the helical type of roll-up further downstream. Subsequently, leaked flows wrap around outside of the leakage vortex formed previously from upstream. The core of leakage vortex thus becomes more distant from the suction side, and the helical type of vortex roll-up grows greater, according as the leakage vortex passes through the cascade passage. On the contrary, the fluid pathlines passing through the downstream half of the gap just wrap around an existing vortex core without roll-up on their own. The tip vortex also occurs in the tip near the pressure surface downstream half of the blade. Furthermore, even in flow through cascades with the tip clearance, the suction leg of the horseshoe vortex continues on the suction side until it reaches the trailing edge.

4. Conclusion

Numerical analysis has been conducted in order to simulate the characteristics of complex flow through a linear cascade of high performance turbine blade with/without tip clearance by using a pressure-correction based, generalized 3D incompressible Navier-Stokes CFD code (MOSA3D).

The development and generation of horseshoe vortex, passage vortex, leakage vortex, tip vortex within tip clearance, etc. are clearly identified through the present simulation, using the RNG k-ε turbulent model with a wall function method and a second-order linear upwind scheme for convective terms. The present simulation results are consistent with the generally known tendency that occurs in the blade passage and tip clearance. It is found from the present simulation result that, in the case of high performance turbine blade, the suction leg of the horseshoe vortex continues on the suction side until it reaches the trailing edge, even in flow with tip clearance. A three-dimensional model for secondary and leakage flows in linear turbine cascades with/without tip clearance is also suggested from the present simulation results, including the effects of tip clearance height.

Acknowledgment

This study was supported by Korea Research Foundation under the grant No. KRF-99-042-E0005 and the Ministry of Science and Technology (Development of Computer-Aided Simulation Software Technology).

References

Bindon, J. P. and Morphis, G., 1992, "The Development of Axial Turbine Leakage Loss for Two Profiled Tip Geometries Using Linear Cascade Data," *ASME J. Turbomachinery*, Vol. 114, No. 1, pp. 198～203.

Chernobrovkin, A., 1999, *Numerical Simulation of Complex Turbomachinery Flows*, PhD Thesis, The Pennsylvania State University.

Chien, K. Y., 1982, "Predictions of Channel and Boundary Layer Flows with a Low-Reynolds-Number Turbulence Model," *AIAA J*, Vol. 20, No. 1, pp. 33～38.

Cho, H. H., Rhee, D. H. and Choi, J. H., 2001, "Heat/Mass Transfer Characteristics on Turbine Shroud with Blade Tip Clearance," *Annals of the New York Academy of Sciences*, Vol. 934, pp. 281～288.

Gregory-Smith, D. G. and Cleak, J. G. E., 1992, "Secondary Flow Measurements in a Turbine Cascade with High Inlet Turbulence," *ASME J. Turbomach.*, Vol. 114, pp. 173～180.

Hah, C., 1984, "A Navier-Stokes Analysis of Three-Dimensional Turbulent Flows inside Turbine Blade Rows at Design and Off-Design Conditions," *ASME J. Eng. Power*, Vol. 106, pp. 421～429.

Ho, Y. and Lakshminarayana, B., 1994, "Computational Modeling of Three Dimensional Endwall Flow Through a Turbine Rotor Cascade with Strong Secondary Flows," *ASME paper* 94 GT-136.

Klein, A., 1966, "Untersuchungen ber die Einfluss der Zustr mgrenzschicht auf die Sekund rstr mung in den Beschaufelungen von Axialturbinen," *Forsch. Ing.*, Bd 32, Nr 6.

Lakshminarayana, B., 1996, *Fluid Dynamics and Heat Transfer of Turbomachinery*, John Wiley & Sons, Inc.

Langston, L. S., Nice, M. L. and Hooper, R. M., 1977, "Three-Dimensional Flow within a Turbine Cascade Passage," *ASME J. Eng. Power*, Vol. 99, pp. 21~28.

Langston, L. S., 1980, "Cross Flow in a Turbine Cascade Passage," *ASME J. Eng. Power*, Vol. 102, pp. 866~874.

Lee, H. G., 1995, Calculation of Turbulent Flows through Turbine Cascades with and without Tip clearance, PhD Thesis, Seoul National University.

Myong, H. K., Park, H. K. and Jin, E., 1996, "Simulation of Three-Dimensional Turbulent Flows around an Ahmed Body-Evaluation of Finite Differencing Schemes -," *Trans. KSME (B)*, Vol. 20, No. 11, pp. 2589~3597.

Sjolander, S. A., 1997, "Secondary and Tip-Clearance Flows in Axial Turbines: Physics of Tip-Clearance Flows-I," von Karman Institute of Fluid Dynamics, Lecture Series 1997-01.

Tallman, J. and Lakshminarayana, B., 2000, "Numerical Simulation of Tip Leakage Flow in Axial Flow Turbines, with Emphasis on Flow Physics, Part I: Effect of Tip Clearance Height," *ASME Paper*, No. 2000-GT-0514.

Yamamoto, A., 1989, "Endwall Flow/Loss Mechanisms in a Linear Turbine Cascades with Blade Tip Clearance," *ASME J. Turbomach.*, Vol. 111, pp. 264~275.

Yoo, J. Y. and Yun, J. W., 1994, "Calculation of a 3D Turbine Cascade Flow," *Computational Mechanics*, Vol. 14, pp. 101~115.